lubricants

MDPI

Article

Hard-Anodized Aluminum Alloy: Wear Properties in Vegetable Oils

Chiara Soffritti, Annalisa Fortini, Enrico Baroni *, Mattia Merlin and Gian Luca Garagnani

Department of Engineering (DE), University of Ferrara, 44121 Ferrara, Italy; chiara.soffritti@unife.it (C.S.); annalisa.fortini@unife.it (A.F.); mattia.merlin@unife.it (M.M.); gian.luca.garagnani@unife.it (G.L.G.)
* Correspondence: enrico.baroni@unife.it

Abstract: The present study examines the tribological behavior of an EN AW-4006 aluminum alloy subjected to two innovative hard anodizing processes involving the sealing of anodic oxide pores with Ag^+ ions and tested in lubricated conditions. Four plant-based lubricants with different concentrations of fatty acids were considered. Wear tests were conducted using a ball-on-disk tribometer, employing a constant frequency oscillatory motion at 2 Hz and a maximum linear speed of 0.1 m/s. The investigation explores the influence of applied loads (5 N, 10 N, and 15 N) on the resulting coefficient of friction. Through a Design of Experiments methodology, the most influential factors affecting the coefficient of friction are identified. The results indicate that hard anodizing processes and applied load affect the coefficient of friction during wear testing as the main factor of influence. High values of the Unsaturation Number led to a high coefficient of friction at 5 N. Wavy-shaped profile tracks were detected at 10 and 15 N, leading to high specific wear rate values and the failure of the anodized layer.

Keywords: aluminum alloy; hard anodizing; friction; wear; vegetable oils

1. Introduction

Aluminum (Al) alloys are employed extensively across a wide range of applications, due to their distinctive low density, high specific strength, and exemplary thermal conductivity and corrosion resistance. However, their unsatisfactory low hardness and poor sliding wear resistance limit their applications and make them hard to use in parts such as aircraft, pneumatic cylinders, and valve components [1–3].

Over recent decades, several surface engineering techniques have been developed to improve the tribological characteristics of Al alloys [4]. The hard anodizing treatment is one of the most cost-effective and diffused electrochemical surface treatments for aluminum and its alloys [5]. The process promotes the growth of a hard and well-compacted Al oxide layer which consists of a thin and pore-free layer in direct contact with the Al substrate, known as a barrier layer, and an outer, thicker, nanoporous layer. The barrier layer is responsible for the corrosion resistance of the anodic oxide layer, while the intrinsic porous nature of the outer layer makes the film poorly resistant to corrosion in aggressive environments [6,7]. A physical or chemical sealing step can be performed as the last step of the anodizing process to reduce the porosity and, consequently, maximize the corrosion resistance of the layer, reduce the adsorption capacity and preserve the aesthetic [8,9]. Anodic oxide layers produced on Al alloys have increasingly attracted much interest due to the regular arrangement of its natural nanoporous pattern, which can be easily controlled and customized by regulating process parameters of the anodizing bath such as the temperature, voltage, and chemical composition [10,11].

Due to their better wear resistance, the dry sliding behavior of conventional and hard anodized layers on commercially pure Al (1XXX series) [12,13], Al-Mg-Si (6XXX series) [2,3], and Al-Zn-Mg (7XXX series) alloys [14,15] have been deeply investigated. Conversely, a lack of scientific papers dealing with the wear resistance of hard anodized layers under

check for updates

Citation: Soffritti, C.; Fortini, A.; Baroni, E.; Merlin, M.; Garagnani, G.L. Hard-Anodized Aluminum Alloy: Wear Properties in Vegetable Oils. *Lubricants* **2024**, *12*, 383. https://doi.org/10.3390/lubricants12110383

Received: 31 August 2024
Revised: 29 October 2024
Accepted: 3 November 2024
Published: 5 November 2024

lubricated conditions can be found in the literature, with most of the works being focused on the filling of the outer nanoporous layer. In fact, the nanopores of the anodic oxide layer can act as reservoirs for functional particles or lubricants to enhance the self-lubricating capability of the surface in sliding contacts. Many researchers investigated the impregnation of the outer nanoporous layer with metallic [16,17] and non-metallic [18–20] particles to obtain functional self-lubricating coatings and maximize the wear resistance of anodized aluminum alloys. Among the proposed solutions, in recent years, the G.H.A.® (Golden Hard Anodizing) process has been developed by G.H.A. Europe S.r.l. (Zola Predosa, Italy). This peculiar hard anodizing treatment involves the presence of silver ions (Ag^+) in a sulfuric acid bath to fill the nanopores of the anodic oxide layer. At present, only a few works deepen the self-lubricating effect of silver on the tribological behavior of the G.H.A.® layers [21,22]. Soffritti et al. [23] investigated the friction and wear resistance of the EN AW-6060 aluminum alloy, which underwent G.H.A.® treatment and traditional hard anodizing in a conventional sulfuric acid bath under varying process conditions. Anodized layers with three different thicknesses—equal to 25, 50, and 100 µm—were examined. Wear tests were conducted in dry conditions, under a normal load of 10 N, at a sliding speed of 0.1 m/s, and using a 100Cr6 steel disk as a counterbody. The results indicated that the 50 µm-thick G.H.A.® anodic oxide layers, which included a sealing step at a temperature below 100 °C, exhibited the lowest coefficient of friction (COF) and specific wear rate (WR) due to their superior adhesion strength. Santecchia et al. [24] studied the wear behavior of an EN AW-6082 Al alloy treated by the G.H.A.® anodizing process with different resulting thicknesses: 10, 50, and 100 µm. Ball-on-disk wear tests were conducted using 100Cr6 and Si_3N_4 as counterparts to evaluate the influence of the thickness of the layer on COF, WR, and on the main wear mechanisms. The authors demonstrated that a 10 µm-thick anodic oxide layer led to the lowest COF against the bearing steel because of a compacted transfer layer of steel debris. Conversely, the highest WR was obtained against Si_3N_4 when the thickness of the anodic oxide layer was 50 µm. Finally, Nastruzzi et al. [25] provided an insight into the anti-microbial properties of the G.H.A.® treatment, proving its appreciable bactericidal efficacy against *Escherichia coli* and *Staphylococcus aureus*. The same authors also offered a tribological characterization of 10 µm-, 25 µm-, and 40 µm-thick G.H.A.® layers on an AA6082 Al alloy, under dry sliding and by using 100Cr6 balls as counterbodies.

Considering the increasingly stringent regulations regarding environmental protection and pollution, the use of mineral and synthetic oils is increasingly being questioned from an environmental sustainability perspective [26,27]. Vegetable oils are preferable as base oils for lubricants because of their renewability, lower toxicity and biodegradability [28,29]. Most vegetable oils mainly consist of triglycerides, i.e., glycerol molecules with three long chains of polar fatty acids attached to the hydroxy groups [30]. Fatty acids in vegetable oils have similar lengths between 14 and 22 atoms of carbon with varying degrees of unsaturation, i.e., the number of double bonds in the C-atoms chain. The polar nature of the fatty acid molecules encourages them to interact with metallic surfaces, generating lubricant monolayer films that are able to reduce both friction and wear. In light of this, vegetable oils are suitable for use in contacts under boundary lubrication conditions [30,31]. Several studies on the tribological properties of vegetable oils, both pure and blended, have been conducted through ball-on-disk/plate [32,33], pin-on-disk [31], and four-ball [30,34] wear tests against metallic surfaces. Conversely, to the best of the authors' knowledge, no works could be found regarding the friction and wear resistance of hard anodized layers lubricated with vegetable oils, despite their non-toxicity and biocompatibility [11].

Based on the results of the above-mentioned literature, the present work deals with the tribological characterization of hard anodized EN-AW-4006 alloy in lubricated conditions and under different normal loads. Especially, the wear properties of two different G.H.A.® processes were investigated through ball-on-disk reciprocating tests using four types of vegetable oils as lubricants. The properties of each natural oil, such as the fatty acid composition, viscosity, and density, were also considered to better understand which conditions can enhance the tribological behavior of the anodic oxide layers under the three

different loads. At last, the main wear mechanisms were examined through a scanning electron microscope operating in variable pressure conditions and equipped with an energy dispersive microprobe for semi-quantitative analysis (VPSEM/EDS).

The value of this scientific article lies in its efforts to enhance the comprehension of the potential of the G.H.A.® treatment, which has not been extensively explored in the existing literature. Additionally, the article investigates the tribological properties of the treatment under lubrication with vegetable oils, with the aim of identifying replacements for current synthetic and petroleum-based oils.

2. Materials and Methods

2.1. Anodized Samples

Disks of 75 mm in diameter and 3 mm in thickness were made in EN AW-4006 aluminum alloy with a nominal chemical composition in agreement with the UNI EN 573-3:2024 standard [35]. The disks were hard anodized according to two innovative treatments. Samples labeled as G underwent the G.H.A.® hard anodizing treatment in a sulfuric acid bath, following a galvanostatic process at a constant current density and temperature ranging between 1 and 10 A/dm^2 and 0 and 1 °C, respectively [36]. The resulting anodic oxide layers were then subjected to a sealing process in boiling water (100 °C) for 2 min/µm. The disks named GP were treated following the G.H.A.PLUS hard anodizing treatment, which involves the above-described G.H.A.® process, but followed by a hydrothermal sealing step in hot water (96 °C) for 2 min/µm to enhance the corrosion resistance of the anodized layer. The designation of the innovative hard anodizing treatments considered in this work, together with a summary of the related sealing parameters, is reported in Table 1.

Table 1. Designation of the innovative hard anodizing treatments considered in this work, together with a summary of the related sealing parameters.

Designation	Anodizing Treatment	Sealing Parameters
G	G.H.A.®	100 °C for 2 min/µm
GP	G.H.A.PLUS	96 °C for 2 min/µm

Roughness parameters (Ra, Rq, and Rz) were measured using a Talysurf CCI Lite non-contact 3D profilometer (Taylor-Hobson, Leicester, UK) to ensure that, before wear tests, all anodized layers presented comparable surface morphology. Five measurements were performed on each anodized surface.

Disks were sectioned to obtain representative cross-sections, oriented perpendicularly to the coating surface. These sections were embedded in epoxy resin and subjected to standard metallographic preparation consisting of grounding with SiC abrasive papers ranging from 120 to 1200 grit, followed by polishing with diamond-based water suspensions. The average thickness of the anodized layers was measured using a Leica DMi8 A optical microscope (Leica, Wetzlar, Germany). For each anodized sample, at least five thickness measurements were taken from five distinct micrographs.

Microhardness tests were performed on the cross-sections by a Vickers Future-Tech FM-110 (Future-Tech Corp., Kawasaki, Japan) hardness tester. A load of 10 gf was applied for a 15 s dwelling time. The average values and the related standard deviations were derived from ten measurements on each anodic oxide layer.

2.2. Vegetable Oils

Four commercially available vegetable oils were chosen to investigate their influence on the tribological performance of the anodized EN AW-4006 alloy: olive, soybean, peanut, and sunflower. They were selected as four of the most widespread natural oils in the world and because of their different composition in terms of saturated and unsaturated fatty acids [37]. Each oil was analyzed by gas chromatography–tandem mass spectrometry (GC-

MS/MS) to obtain the specific contents of fatty acid molecules. The degree of unsaturation of the different vegetable oils was subsequently obtained by determining the Unsaturation Number (UN). Starting from the general form of the equation [38], this parameter was calculated as shown in Equation (1):

$$UN = \frac{1}{100}\{[1 \times (C16:1 + C18:1 + C20:1 + C22:1)] + [2 \times (C18:2 + C22:2)] + [3 \times (C18:3)]\} \quad (1)$$

where *Cx:y* is the percentage of the fatty acid in the natural oil, *x* is the length of the carbon (C) atoms chain, and *y* is the number of double bonds.

The dynamic viscosity of the oils was measured by a Rheometric Scientific ARES-LS (TA Instruments, New Castle, DE, USA) rotational rheometer equipped with 25 mm titanium parallel disks with a gap between the plates set to 1 mm. Measurements were repeated three times for each vegetable oil, with a shear rate in the range 1 to 100 s^{-1}, and at three different temperatures (25, 40, and 100 °C), following the methodology reported by Georgescu et al. [37]. The Viscosity Index of each fluid was then calculated according to the ASTM D2270 standard as a function of the kinematic viscosity of the vegetable oil at 40 and 100 °C [39].

The density of the vegetable oils was determined by filling four cylinders, with a capacity of 100 mL and uncertainty of 0.5 mL, with 10 mL of oil. The cylinders (one for each type of vegetable oil) were weighed in turn on a Kern ABT 100-5NM analytical balance (Kern, Balingen, Germany). Each weight was then converted into density by dividing it for the oil volume. Five measurements were conducted for each vegetable oil.

2.3. Tribological Tests

Lubricated tribological tests were conducted in ball-on-disk configuration at room temperature (~25 °C and constant) using a TR-20 LE (Ducom Instruments, Bangalore, India) tribometer. Balls of 10 mm in diameter made of 100Cr6 steel were chosen as counterbodies against the anodized disks. Reciprocating wear tests at a constant motion inversion frequency of 2 Hz (corresponding to an average sliding speed of 0.1 m/s) were performed in triplicate. The stroke length and the total sliding distance were set equal to 25 mm and 250 m, respectively, according to previous work published by the authors [23]. Three different normal loads equal to 5, 10, and 15 N were considered to evaluate the effects of this parameter on the tribological behavior of both vegetable oils and anodized layers. Before wear tests, disks and balls were ultrasonically bathed with isopropanol for 2 min to avoid contamination between different oils. The coefficient of friction was monitored and registered during each test by the instrument and the steady state mean value was calculated upon the three replicas of each condition after 25 m of the sliding motion. The tribological tests were performed randomly in accordance with the Design of Experiments (DoE) methodology to avoid the influence of external uncontrollable factors. A full-factorial design was adopted to investigate the main factors of influence on the COF. The main factors and corresponding levels for the application of DoE methodology are summarized in Table 2.

Table 2. Main factors and corresponding levels for the application of DoE methodology.

Factors	**Levels**			
Anodized layer	G	GP	-	-
Normal load [N]	5	10	15	-
Vegetable oil	Olive	Soybean	Peanut	Sunflower
N. of replicas	3			

Friction regimes were classified at each investigated condition by calculating the respective dimensionless ratio λ according to the following Equation (2):

$$\lambda = \frac{h_{min}}{\sqrt{\left({R_{q1}}^2 + {R_{q2}}^2\right)}} \quad (2)$$

where h_{min} is the minimum film thickness and R_{q1} and R_{q2} are the root mean square roughness values for the two mating surfaces [40]. According to Hamrock et al. [41], the minimum film thickness, h_{min}, can be calculated in cases of point contact through the following Equation (3):

$$h_{min} = 3.63 \cdot U^{0.68} \cdot G^{0.49} \cdot R \cdot W^{-0.073} \cdot \left(1 - e^{-0.68k}\right) \quad (3)$$

in which U is the non-dimensional speed parameter, G is the non-dimensional materials parameter, R is the reduced radius of curvature, W is the non-dimensional load parameter, and k is the non-dimensional ellipticity parameter. The central film thickness, h_c, was calculated through the model proposed by the same authors following Equation (4):

$$h_c = 2.69 \cdot U^{0.67} \cdot G^{0.53} \cdot R \cdot W^{-0.067} \cdot \left(1 - 0.61e^{-073k}\right) \quad (4)$$

The reduced equivalent elastic modulus of the anodized Al alloy, which considers both the mechanical properties of the Al substrate and anodic oxide layer, was obtained according to the method proposed by Liu et al. [42]. For the above-mentioned calculation, the mechanical properties and roughness parameter Rq of the different materials involved in the Hertzian contact under examination were collected in Table 3.

Table 3. Mechanical properties and roughness parameter Rq of the different materials involved in the Hertzian contact under examination.

	Young Modulus [GPa]	Poisson's Ratio	Rq [µm]
100Cr6 (ball)	210 [1]	0.30 [1]	0.03 [1]
EN AW-4006 (disk/substrate)	69 [2]	0.33 [2]	*Useless*
Anodic oxide layer (disk/coating)	90 [3]	0.24 [3]	*Measured*

[1] according to Ortega-Alvaréz et al. [43]. [2] estimated from data sheets provided by the suppliers. [3] according to Tsyantsaru et al. [12].

The wear tracks on the disks were analyzed through the same Talysurf CCI Lite non-contact 3D profilometer (Taylor-Hobson) to evaluate the cross-section area of the wear track. At least five measurements were performed along the track to calculate the volume of the worn material. The specific wear rate (WR) was then obtained as the ratio between the volume loss and the product of the sliding distance and the applied load [44].

A ZEISS EVO MA 15 (Zeiss, Oberkochen, Germany) scanning electron microscope operating in variable pressure conditions and coupled with an Oxford X-Max 50 (Oxford Instruments, Abingdon-on-Thames, UK) microprobe for energy-dispersive spectroscopy (VPSEM/EDS) was used to analyze the worn surface of the anodized disks and to investigate the main wear mechanisms.

3. Results & Discussion

3.1. Anodized Samples

The optical micrographs in the cross-section of the anodized layers before wear tests are reported in Figure 1. The anodic oxide layers are similar due to the same anodizing bath they underwent. As already observed in the literature [17,45], both barrier and nanoporous layers, normally composed of aluminum hydroxide, cannot be distinguished due to their

very low thickness. The yellow arrows in the figure also indicate uniformly distributed voids and macro-pores, as a result of incorporation within the coating of the secondary phases in the EN AW-4006 substrate [46]. In this regard, Scampone et al. [47] stated that Fe-rich intermetallics may be partially or totally dissolved during anodizing, causing voids and defects in the anodic oxide layer.

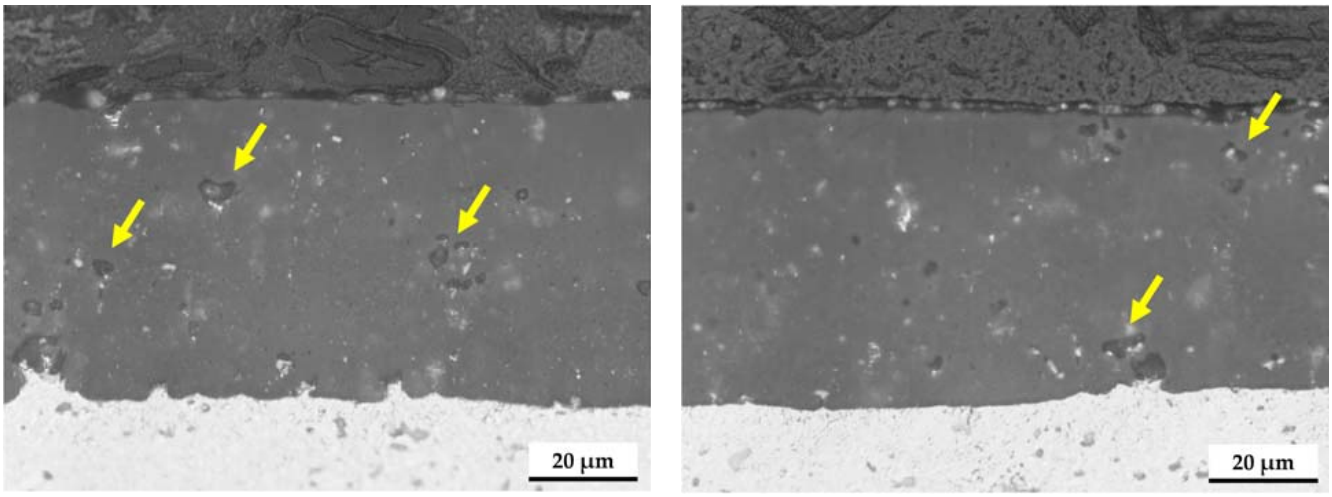

G **GP**

Figure 1. Optical micrographs in the cross-section of the anodized layers before wear tests. The yellow arrows indicate uniformly distributed voids and macro-pores.

Table 4 collects the mean values and related standard deviations of thickness, Vickers microhardness (HV0.01), and roughness parameters (Ra, Rq, Rz) of the different anodic oxide layers. All anodized layers show similar values of the above-mentioned parameters, which are also slightly higher than those previously reported for G.H.A.® layers [23].

Table 4. Thickness, Vickers microhardness (HV0.01), and roughness parameters (Ra, Rq, Rz) of the different anodic oxide layers.

	Thickness [µm]	HV0.01	Ra [µm]	Rq [µm]	Rz [µm]
G	56 ± 1	494 ± 28	0.48 ± 0.02	0.65 ± 0.03	4.28 ± 0.38
GP	53 ± 2	500 ± 35	0.48 ± 0.06	0.64 ± 0.08	4.10 ± 0.92

3.2. Vegetable Oils

The saturated and unsaturated fatty acid contents, Unsaturation Number (UN), and mean values ± standard deviations of the density of the vegetable oils adopted in this work are reported in Table 5. Soybean and sunflower oils show high UN (1.5059 and 1.4873, respectively) because of the high contents of linoleic fatty acid (C18:2). On the other hand, olive and peanut oil exhibit low UN values (0.9635 and 0.9468, respectively) given their high oleic acid contents (C18:1). In the case of olive oil, the highest content of the saturated palmitic acid (C16:0) was also detected. All vegetable oils showed similar mean densities, being higher than those reported in the field literature [31,48]. Based on the results of the shear viscosity reported in Figure 2, kinematic viscosity was calculated, and based on that value, the viscosity index was obtained according to ASTM D2270. All the vegetable oils presented a high viscosity index, as already deeply studied in the literature, [31]. Peanut oil was characterized by the lowest value, meaning a quicker viscosity decrease while increasing the temperature.

Table 5. Saturated and unsaturated fatty acid contents, Unsaturation Number (UN), and mean values ± standard deviations of the density of the adopted vegetable oils in this work, together with their respective Viscosity Indexes.

	Saturated Fatty Acids		Unsaturated Fatty Acids									
Vegetable Oil	**C16:0**	**C18:0**	**C16:1**	**C18:1**	**C20:1**	**C22:1**	**C18:2**	**C22:2**	**C18:3**	**UN**	**Density [g/cm^3]**	**Viscosity Index**
Olive	0.1205	0.0274	0.0086	0.7186	0.0031	0.0000	0.1055	0.0000	0.0074	**0.9635**	**0.942 ± 0.001**	**595**
Soybean	0.1072	0.0436	0.0009	0.2432	0.0016	0.0000	0.5230	0.0000	0.0714	**1.5059**	**0.949 ± 0.001**	**592**
Peanut	0.0709	0.0243	0.0013	0.7351	0.0181	0.0000	0.0945	0.0000	0.0011	**0.9468**	**0.948 ± 0.001**	**538**
Sunflower	0.0647	0.0358	0.0010	0.2863	0.0013	0.0000	0.5980	0.0000	0.0009	**1.4873**	**0.936 ± 0.001**	**578**

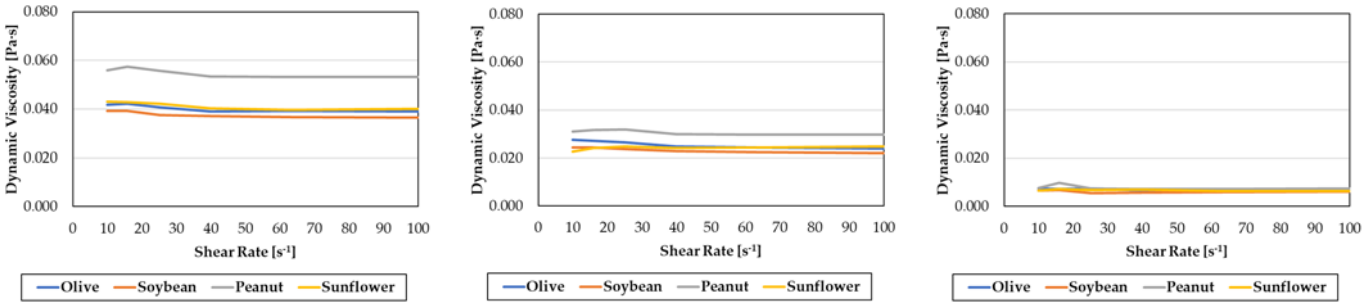

(**a**) 25 °C (**b**) 40 °C (**c**) 100 °C

Figure 2. Dynamic viscosity of the vegetable oils at the three different temperatures: (**a**) 25 °C, (**b**) 40 °C, and (**c**) 100 °C.

In Figure 2, the dynamic viscosity of the considered vegetable oils is reported as a function of the shear rate for the three different temperatures (25, 40, and 100 °C) in the range between 10 and 100 s^{-1}, as in the literature [37]. As a general trend, it can be observed that the dynamic viscosity of all vegetable oils decreases as the temperature at which the viscosity is measured increases. Furthermore, peanut oil shows the highest dynamic viscosity both at 25 and 40 °C. According to the Herschel–Bulkley model [49], a classification of the oils is possible after a calculation of the yield stress, τ_0, and the flow index, n, through a tailored MATLAB® code [50]. Since all oils, irrespective of the investigated temperature, are characterized by negligible τ_0 values and by n values ranging between 0.96 and 1.06, they could be assumed to be Newtonian fluids. Considering this, the dynamic viscosity may be considered independent of the shear stress.

3.3. Tribological Characterization

The representative COF evolution against the sliding distance at the different applied loads and for a G sample lubricated with olive and peanut oil are reported in Figure 3. For the sake of clarity, the COF evolutions against the sliding distance for all test conditions are reported in Appendix A. Regardless of the selected vegetable oil, at all loads, the COF presented an almost instant increase at the very beginning of the sliding motion. It is then followed by a steady state during which the coefficient of friction shows only slight fluctuations around a lower mean value. As suggested by Blau [51], this behavior is typical for lubricated sliding contact under a boundary lubrication regime until the lubricant meatus is generated. Irrespective of the type of vegetable oils, all tribocouples show the lowest COF at the applied load of 5 N. At 10 and 15 N, the COF is higher, with a small difference between the average values. Comparing the behavior of olive and peanut oils (Figure 3a,b as representative COF variations), it can be noticed that a higher COF mean value was provided from peanut oil when a 5 N load was applied. This can be attributed

to the higher shear viscosity of the peanut oil at room temperature (25 °C) in respect of the one of the olive oils. Increasing the load up to 10 and 15 N, the frictional behavior of peanut oil resulted in the same values as those of the other vegetable oils. An explanation of this general behavior could be provided by the lowest viscosity index of the peanut oil, which led to a quicker degradation of the lubricity properties of the vegetable oil.

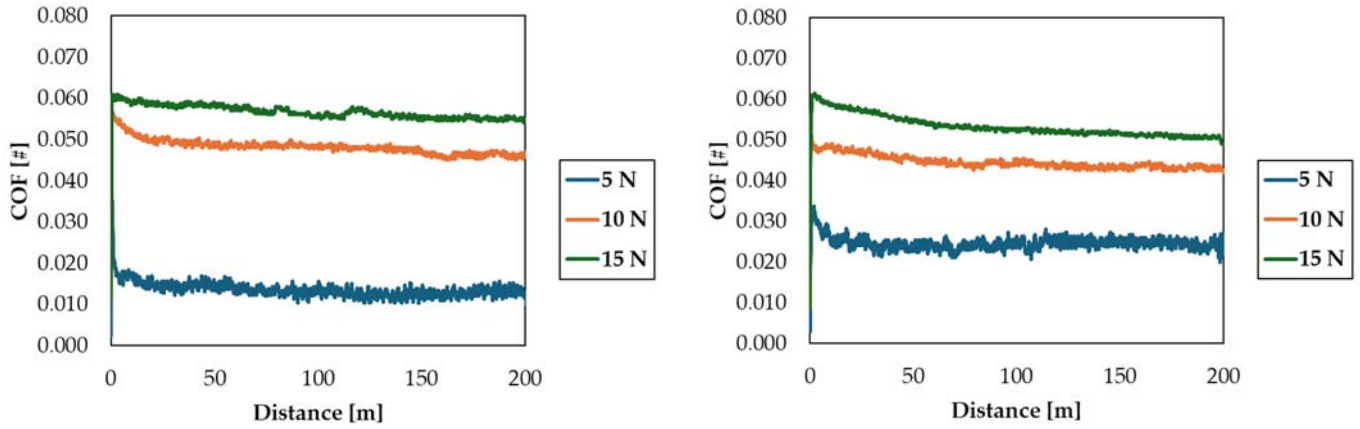

Figure 3. Representative COF evolution against sliding distance at the different applied loads and for a G sample lubricated with (**a**) olive oil and (**b**) peanut oil.

The mean values and related standard deviations of the coefficient of friction at the steady state for all test conditions are shown in Table 6. For all anodized layers, the coefficient of friction increases with the increasing applied load. At 5 N, the highest COF values are shown by GP when soybean is used as the lubricant, while using peanut oil, the highest COF is reached on G samples. In the case of lubrication with olive and sunflower oils, all anodized samples show similar COF values. At applied loads of 10 and 15 N, the influence of the considered vegetable oil seems to be less discernible. To better understand the COF obtained in the different conditions, the results were statistically analyzed through ANOVA in the DoE methodology. The three-factorial design obtained a strong R^2 factor equal to 98.561%, which quantifies the percentage of variation in the response that is explained by the model. Considering the anodized layer as a factor, it was found that G and GP do not provide significant differences in the results. The entity of the normal load turns out to be the main influence effect since a large difference in the results was found between 5 N and 10 N. A similar behavior was observed between 10 and 15 N, though to a lesser degree. Concerning vegetable oil as the main effect, the highest COF mean value was obtained with soybean oil. Lubrication with olive and peanut oils, characterized by a low UN (equal to 0.9635 and 0.9468, respectively), leads to lower COF values than those of soybean oil (UN = 1.5059). On the other hand, using sunflower oil—characterized by high UN and the lowest content of saturated fatty acids—as a lubricant allowed for obtaining the lowest COF.

Analyzing the interaction between different factors, it was also found that, at 15 N, the COF mean value is correlated with the UN variations. Indeed, the higher the UN, the higher the COF, thus confirming previous results in the literature [26,31]. On the contrary, different trends were found at 5 N and 10 N. In the case of the 5 N normal load, the lowest COF values are obtained with peanut oil as a lubricant, while at 10 N, the same oil provided the highest COF mean values. Reeves et al. [31] registered higher COF values for a copper-aluminum alloy tribocouple tested in a pin-on-disk configuration, under a high applied load and sliding speed, and lubricated with many types of vegetable oils. Comparable COF results were obtained by Faes et al. [52] while investigating the effect of fatty acids ionic

liquids on the tribological properties of 100Cr6 steel against a wide selection of metallic and non-metallic surfaces.

Table 6. Mean values and related standard deviations of the coefficient of friction at the steady state for all test conditions.

	G		
	5 N	**10 N**	**15 N**
Olive	0.013 ± 0.003	0.048 ± 0.001	0.056 ± 0.002
Soybean	0.018 ± 0.002	0.050 ± 0.002	0.060 ± 0.001
Peanut	0.024 ± 0.001	0.044 ± 0.003	0.053 ± 0.001
Sunflower	0.017 ± 0.003	0.047 ± 0.002	0.057 ± 0.003
	GP		
	5 N	**10 N**	**15 N**
Olive	0.014 ± 0.003	0.052 ± 0.004	0.056 ± 0.001
Soybean	0.026 ± 0.003	0.046 ± 0.004	0.060 ± 0.002
Peanut	0.023 ± 0.003	0.044 ± 0.002	0.052 ± 0.001
Sunflower	0.018 ± 0.001	0.043 ± 0.001	0.050 ± 0.002

Figure 4 presents the relationship between COF and WR for G and GP anodized layers for each investigated condition according to the interpretation proposed by Guicciardi et al. [53] and widely used in the literature in the case of lubricated sliding contacts [54,55]. As a general trend, it can be observed that the higher the applied load, the higher the dispersion of the COF-WR points, indicating a simultaneous increment of both COF and WR. This effect was less effective in the case of the GP anodized layer (see Figure 4b). However, the same trend was observed in both the tested surfaces, with a considerable degree of scatter between 5 and 10 N and a relatively lower increment between 10 and 15 N. Moreover, in the case of the G anodized layer (see Figure 4a), the higher the applied load, the lower the difference in terms of COF under different vegetable oils' lubrication. Peanut and sunflower oils provided the maximum WR at each test condition, showing the maximum values in the case of the G-anodized disk. Both oils also presented similar values of the ratio between unsaturated and saturated fatty acids due to their lower content of saturated acids.

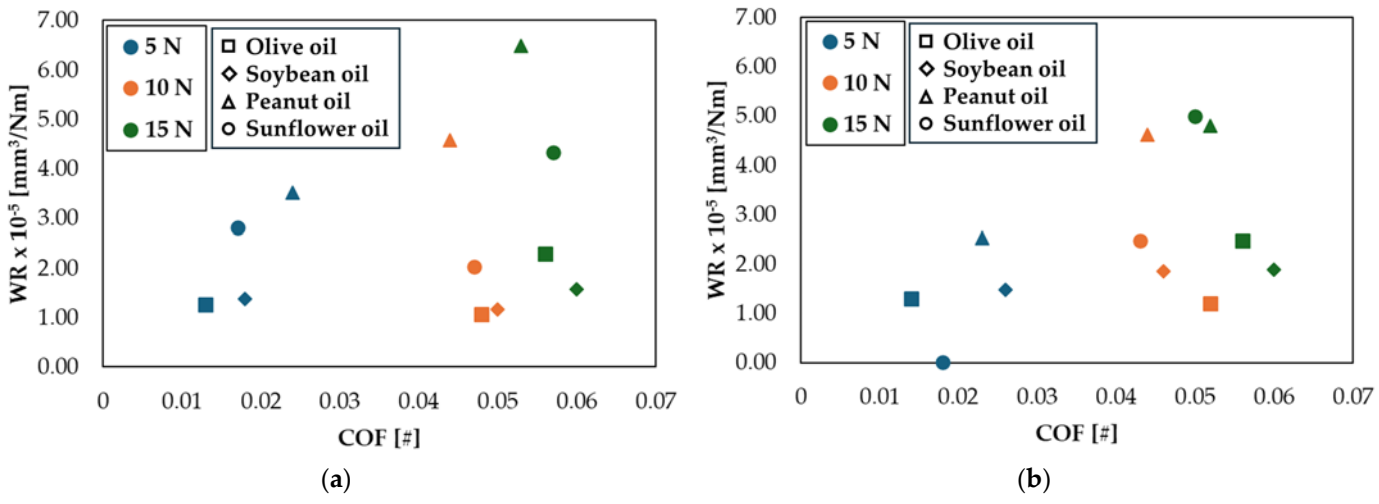

Figure 4. Relationship between COF and their respective WR values for (**a**) G and (**b**) GP anodized layers.

The values of central film thickness (h_c), minimum film thickness (h_{min}), and the λ factor were then calculated to determine the ongoing lubrication regime during the wear tests. The values of the above-mentioned parameters for all test conditions are shown in Table 7. It must be noticed that λ values are reported as a range to take into account the Rq roughness parameters of the two different anodized layers, which determined the lower (when Rq was equal to 0.64 μm) and upper (when Rq was equal to 0.65 μm) end of the range. All λ values are in the range of 0.024 to 0.041, thus suggesting a boundary lubrication regime. The thickest meatus was found when peanut oil was used as a lubricant due to its highest dynamic viscosity (see Figure 2) at each investigated normal load. The subsequent higher distance between the mating surfaces could have caused the lowering of COF, as already detailed during the discussion of data in Table 6.

Table 7. Values of central film thickness (h_c), minimum film thickness (h_{min}) and the λ factor for all test conditions.

		h_c [nm]	h_{min} [nm]	λ
5 N	Olive	25.8	20.5	0.031–0.032
	Soybean	24.5	19.4	0.029–0.030
	Peanut	32.9	26.1	0.040–0.041
	Sunflower	26.3	20.9	0.032–0.033
10 N	Olive	24.7	19.5	0.029–0.030
	Soybean	23.4	18.5	0.028–0.029
	Peanut	31.4	24.8	0.038–0.039
	Sunflower	25.1	19.8	0.030–0.031
15 N	Olive	24.0	18.9	0.028–0.029
	Soybean	22.8	17.9	0.027–0.028
	Peanut	30.5	24.0	0.035–0.037
	Sunflower	24.5	19.3	0.029–0.030

Finally, the mean values and related standard deviations of WR for the anodized layers in all test conditions are reported in Table 8. All samples show similar variations in WR with varying applied loads and vegetable oil, except for the sunflower oil. Indeed, for an applied load of 5 N, the GP disks lubricated with sunflower oil exhibit no evidence of wear damage on their surface. The highest WR values, concurrently with the largest standard deviations, were obtained at normal loads ranging between 10 and 15 N, particularly when peanut and sunflower oils were adopted as lubricants.

To fully understand the wear mechanisms determining COF and WR values for the different investigated cases, the wear tracks on the disks were analyzed through VPSEM/EDS. The representative VPSEM/EDS micrographs of the wear tracks on the anodized layers, after wear tests at the different applied loads, are reported in Figure 5. First of all, the different scales of the micrographs must be noted to better appreciate the proportion of the wear phenomena. Figure 5a,b depict the wear track on the G disk when a 5 N normal load was applied and olive oil was used as lubricant. Wide cracks alongside the sliding direction are found to define the edges of the wear track (white arrows in the figure), but no variations in the superficial topography could be detected. Abedini et al. [17] found similar cracks at the edges of the wear track as a result of the plastic deformation of the anodized layer filled with Ni particles. The same type of wear damage was found on all worn surfaces tested under the same normal load irrespective of the vegetable oils.

Table 8. Mean values and related standard deviations of the specific wear rate [10^{-5} $mm^3/(N \cdot m)$] for the anodized layers in all test conditions.

	G		
	5 N	**10 N**	**15 N**
Olive	1.25 ± 0.13	1.06 ± 0.20	2.28 ± 0.43
Soybean	1.37 ± 0.43	1.16 ± 0.13	1.57 ± 0.46
Peanut	3.50 ± 1.38	4.56 ± 3.15	6.47 ± 1.31
Sunflower	2.82 ± 1.35	2.03 ± 1.53	4.33 ± 1.80
	GP		
	5 N	**10 N**	**15 N**
Olive	1.29 ± 0.34	1.20 ± 0.13	2.47 ± 0.47
Soybean	1.48 ± 0.64	1.85 ± 0.34	1.88 ± 0.05
Peanut	2.52 ± 1.25	4.61 ± 1.76	4.79 ± 0.69
Sunflower	-	2.48 ± 2.43	5.00 ± 4.28

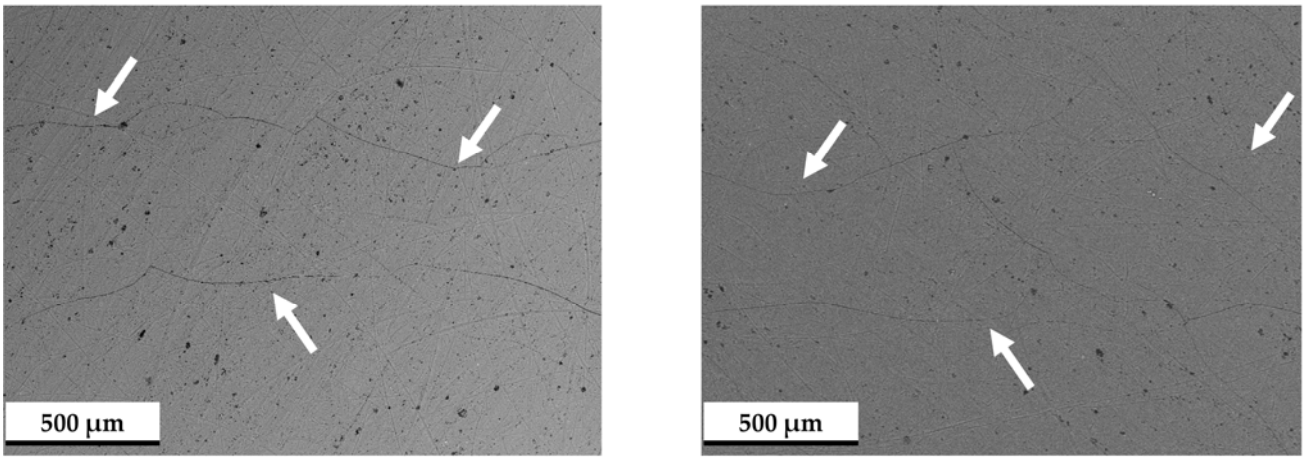

(**a**) (**b**)

Figure 5. Representative VPSEM micrographs of the wear tracks on the anodized layers after wear tests at applied loads of 5 N for (**a**) G and (**b**) GP samples. The white arrows show wide cracks alongside the sliding direction.

On the other hand, at 10 N and 15 N, a different surface morphology was observed on the wear tracks, which appeared with a wavy-shaped profile, as depicted in Figure 6. Especially, these profiles were found to be constituted by an alternation of pile-up and depressed areas with circular edges both in the case of G and GP anodized layers. The main wear mechanism seemed to be the same for both anodized layers at 10 and 15 N, with wide cracks alongside the direction of reciprocating sliding (see Figure 6a,b) and thicker cracks longitudinal and transverse to the sliding direction (red circle in Figure 6c,d). The yellow arrows in the figure highlight a number of cracked junctions between the zones. The causes of such behavior may be different. One of the biggest limitations associated with using vegetable oils as lubricants includes their poor oxidation stability, which depends on their number of unsaturated fatty acids [56,57]. Oxidation can deteriorate the lubricity effect of vegetable oils, determining high COF and WR [58]. The decaying effectiveness of these oils combined with the thinning of the meatus could have determined an increase in the extent of contact between mating surfaces. Similar wavy-shaped profiles of the wear tracks were also found by Bahari et al. [26] while investigating the friction and wear resistance of a grey cast iron coupled with 100Cr6 steel balls, after reciprocating ball-on-flat wear tests under lubrication with palm and soybean oils and their blends. The authors

demonstrated that the contact pressure between the mating surfaces overstepped the shakedown limit, determining plastic ratcheting [59,60]. This phenomenon causes, in turn, the plastic deformation of the softer material during cyclic sliding. The alternation of pile-up and depressed areas also seems to explain the large standard deviation of the WR in the case of applied loads equal to 10 and 15 N (see Table 8). The different wear mechanism agrees with the findings shown in Figure 4, in which the worst wear resistance of the coatings was obtained at the highest loads.

A representative VPSEM micrograph showing the detail of the cracked wavy-shaped profile of the worn anodized layers after wear tests at the highest loads is depicted in Figure 7, together with semi-quantitative EDS analysis at different positions on the wear track. The elemental composition of the light grey zone (blue arrow) revealed the presence of a high concentration of Al and traces of Si and Fe. This finding proves the failure of the anodic oxide layers by chipping, similar to that reported by Kwolek et al. in [61]. The EDS semi-quantitative analysis of the positions denoted by the red arrows also revealed the presence of Ag-rich particles as additional evidence of the failure of the coating.

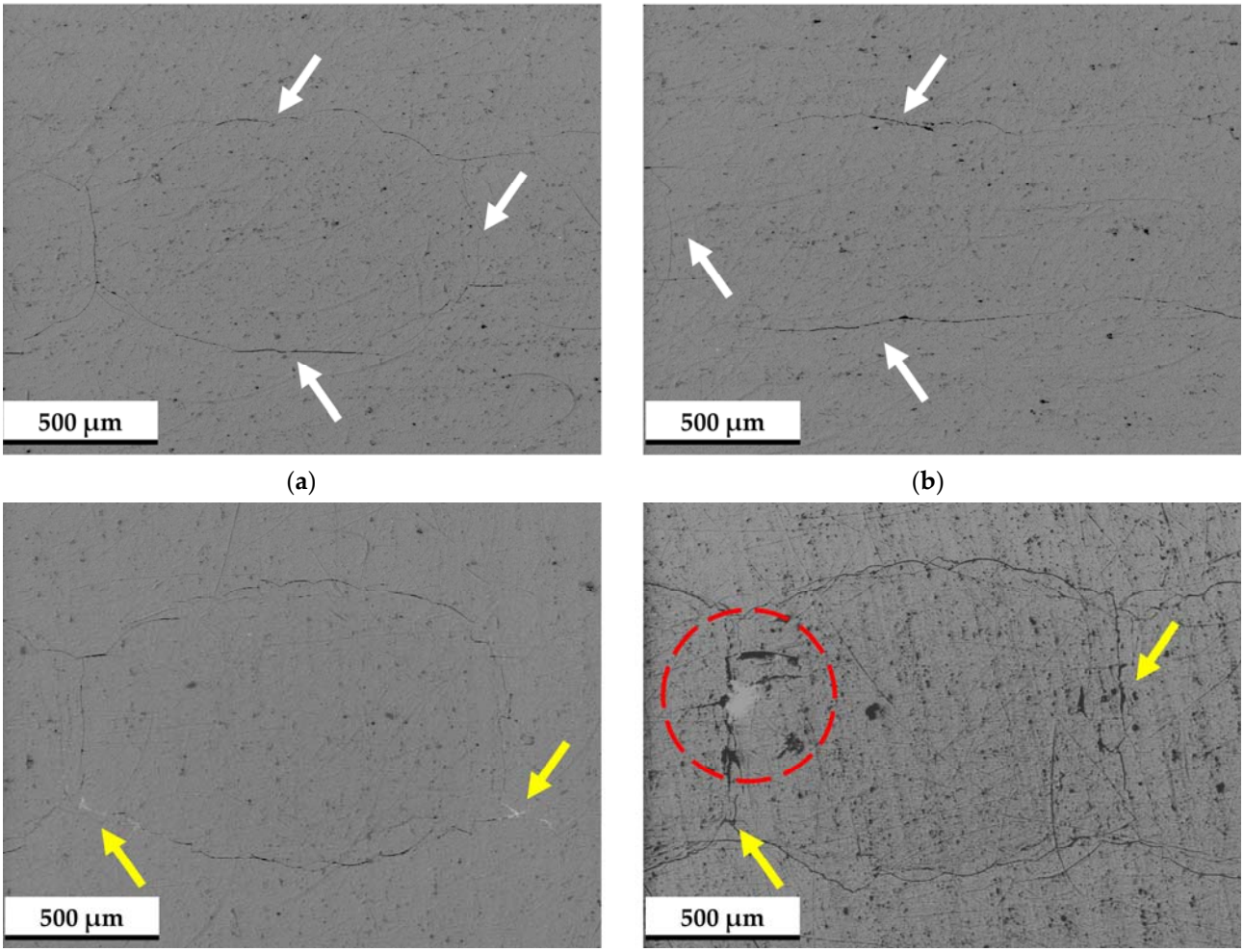

Figure 6. Representative VPSEM micrographs of the wear tracks on the anodized layers after wear tests at applied loads of (**a**,**b**) 10 N and (**c**,**d**) 15 N. (**a**,**c**) refer to G wear tracks obtained under sunflower oil lubrication. (**b**,**c**) refer to GP wear tracks obtained under sunflower oil lubrication. The white arrows in (**a**,**b**) show wide cracks alongside the sliding direction. In (**c**,**d**), the yellow arrows indicate cracked junctions between depression zones, whereas the red circle shows thick cracks longitudinal and transverse to the sliding direction.

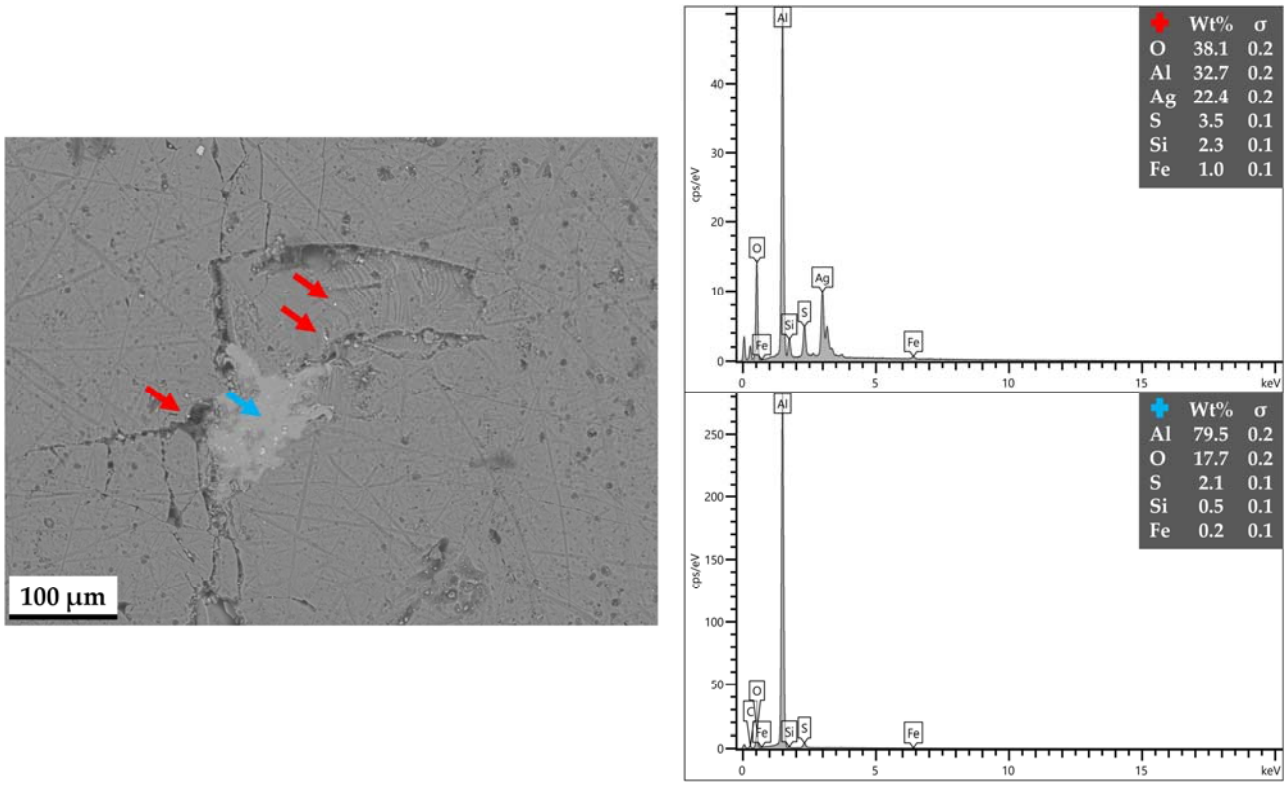

Figure 7. Representative VPSEM micrograph showing the detail of the cracked wavy-shaped profile of the worn anodized layers after wear tests at the highest loads, together with semi-quantitative EDS analysis at different positions (blue and red arrows) of the wear track.

4. Conclusions

In the present work, the tribological properties of the EN AW-4006 Al alloy treated by the innovative G.H.A.® hard anodizing process were investigated in the case of lubrication with vegetable oils. The influence of olive, soybean, peanut, and sunflower vegetable oils was considered, together with the effect of different normal loads (5, 10, and 15 N). The coefficient of friction, specific wear rate, and main wear mechanisms were investigated to better comprehend the tribological behavior. Based on the results, the following conclusions can be drawn:

- The two different sealing procedures did not affect the properties of G and GP anodized layers. Similar thickness values, Vickers microhardness values, and roughness parameters were obtained.
- The COF values followed different trends at the investigated normal loads. When a 15 N load was applied, the higher the UN of the vegetable oil, the higher the COF. At loads equal to 5 and 10 N, lubrication with peanut oil determined the lowest and the highest average values of the coefficient of friction, respectively.
- Two different tribological behaviors were suggested by WR values. The lowest values of the WR were obtained for G and GP samples using olive and soybean oils at each applied load, while peanut and sunflower oils determined the highest WR. The large standard deviations at 10 and 15 N suggested irregular-shaped wear tracks.
- Concerning wear mechanisms, at 5 N, wide longitudinal cracks along the sliding direction were detected as a result of the plastic deformation of the anodized layers. On the other hand, wavy-shaped profiles were found on the wear tracks at 10 and 15 N. These profiles were constituted by an alternation of pile-up and depressed areas with circular edges with cracked junctions.

Author Contributions: Conceptualization, C.S. and A.F.; methodology, C.S.; software, E.B.; validation, C.S., M.M. and G.L.G.; formal analysis, M.M.; investigation, C.S., E.B., A.F. and M.M.; resources, A.F.; data curation, C.S. and E.B.; writing—original draft preparation, E.B.; writing—review and editing, C.S., A.F. and M.M.; visualization, C.S. and E.B.; supervision, G.L.G. and M.M.; funding acquisition, M.M. and G.L.G. All authors have read and agreed to the published version of the manuscript.

Funding: This research was funded by FAR 2024 funding from the University of Ferrara (Ferrara, Italy), aimed at the tribological characterization of wrought aluminum alloys treated by innovative hard anodizing treatments involving the sealing of anodic oxide pores with silver ions.

Data Availability Statement: The raw data supporting the conclusions of this article will be made available by the authors on request.

Acknowledgments: The authors gratefully acknowledge G.H.A. Europe s.r.l. for supplying the materials and the anodizing treatments investigated in this work. The authors also wish to thank Franco Cicerchia, Eng. Costantino Cicerchia and Alessandro Savelli for the technical assistance. The authors would like to acknowledge Eng. Nicola Zanini and Eng. Valentina Mazzanti for the support during the vegetable oils characterization. The authors would also like to thank Eng. Elia Mantovani for the support during the tribological investigations.

Conflicts of Interest: The authors declare no conflicts of interest.

Appendix A

In this section, the coefficient of friction (COF) evolutions against the sliding distance for all test conditions are reported. It should be noted that Figure 3a,b are also reported, showing the representative COF evolution against the sliding distance at the different applied loads and for G samples lubricated with olive and peanut oils.

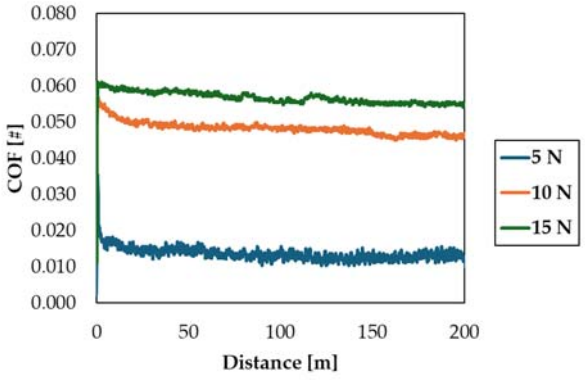

G—Olive oil (see Figure 3a)

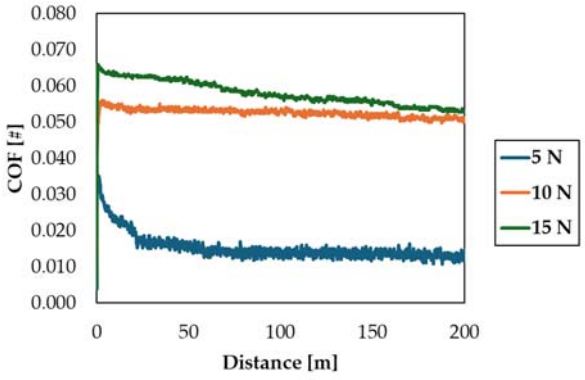

GP—Olive oil

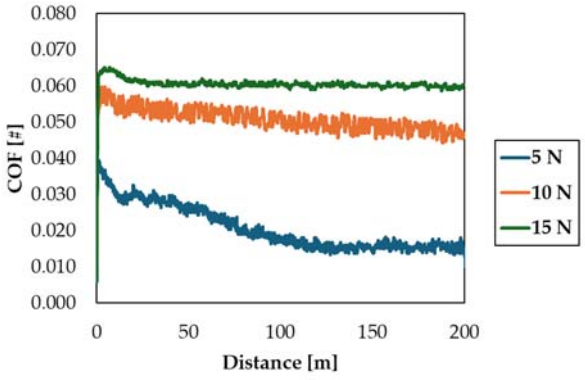

G—Soybean oil

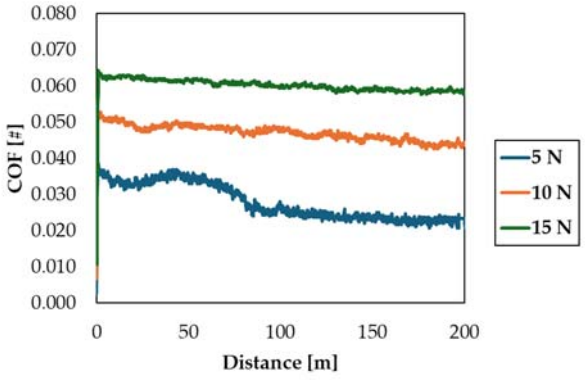

GP—Soybean oil

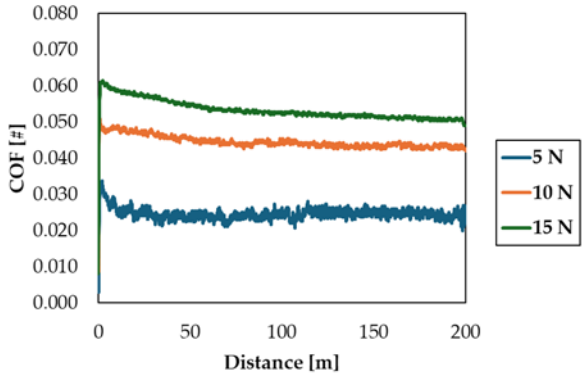

G—Peanut oil (see Figure 3b)

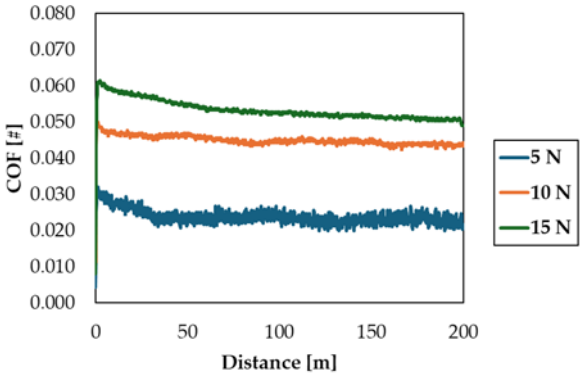

GP—Peanut oil

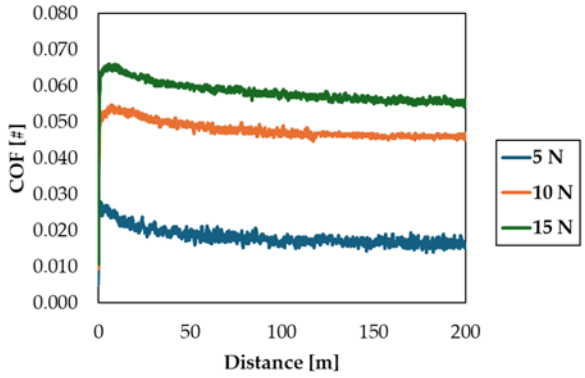

G—Sunflower oil

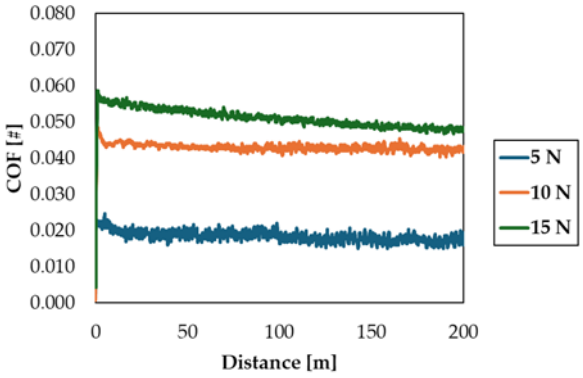

GP—Sunflower oil

References

1. Rajasekaran, B.; Ganesh Sundara Raman, S.; Rama Krishna, L.; Joshi, S.V.; Sundararajan, G. Influence of Microarc Oxidation and Hard Anodizing on Plain Fatigue and Fretting Fatigue Behaviour of Al-Mg-Si Alloy. *Surf. Coat. Technol.* **2008**, *202*, 1462–1469. [CrossRef]
2. Sola, R.; Tonelli, L.; Shashkov, P.; Bogdanoff, T.H.; Martini, C. Anodizing of AA6082-T5 by Conventional and Innovative Treatments: Microstructural Characterization and Dry Sliding Behaviour. *Wear* **2020**, *458–459*, 203423. [CrossRef]
3. Mohitfar, S.H.; Mahdavi, S.; Etminanfar, M.; Khalil-Allafi, J. Characteristics and Tribological Behavior of the Hard Anodized 6061-T6 Al Alloy. *J. Alloys Compd.* **2020**, *842*, 155988. [CrossRef]
4. Cotelli, C.M.; Sprague, J.A.; Smidt, F.A., Jr. Surface Engineering of Aluminum and Aluminum Alloys. In *Surface Engineering*; ASM International: Novelty, OH, USA, 1994; Volume 5, pp. 784–804.
5. Kwolek, P. Hard Anodic Coatings on Aluminum Alloys. *Adv. Manuf. Sci. Technol.* **2017**, *41*, 35–46. [CrossRef]
6. Zhang, X.X.; Jin, Y.X.; Wang, H.P.; Yang, Y. Development and Application of Porous Anodic Alumina Template. *Appl. Mech. Mater.* **2013**, *320*, 558–566. [CrossRef]
7. Caliari, D.; Timelli, G.; Zabala, B.; Igartua, A. Microstructural and Tribological Investigations of Diecast and Hard Anodized AlSiCu Alloys. *Surf. Coat. Technol.* **2018**, *352*, 462–473. [CrossRef]
8. Shang, Y.; Wang, L.; Liu, Z.; Niu, D.; Wang, Y.; Liu, C. The Effects of Different Sealing Techniques for Anodic Film of Al-12.7Si-0.7Mg Alloys. *Int. J. Electrochem. Sci.* **2016**, *11*, 5234–5244. [CrossRef]
9. Ono, S.; Asoh, H. Mechanism of Hot Water Sealing of Anodic Films Formed on Aluminum. *Corros. Sci.* **2021**, *181*, 109221. [CrossRef]
10. Mehdizade, M.; Soltanieh, M.; Eivani, A.R. Investigation of Anodizing Time and Pulse Voltage Modes on the Corrosion Behavior of Nanostructured Anodic Layer in Commercial Pure Aluminum. *Surf. Coat. Technol.* **2019**, *358*, 741–752. [CrossRef]
11. Dobosz, I. Influence of the Anodization Conditions and Chemical Treatment on the Formation of Alumina Membranes with Defined Pore Diameters. *J. Porous Mater.* **2021**, *28*, 1011–1022. [CrossRef]
12. Tsyntsaru, N.; Kavas, B.; Sort, J.; Urgen, M.; Celis, J.P. Mechanical and Frictional Behaviour of Nano-Porous Anodized Aluminium. *Mater. Chem. Phys.* **2014**, *148*, 887–895. [CrossRef]
13. Hu, N.-N.; Ge, S.-R.; Fang, L. Tribological Properties of Nano-Porous Anodic Aluminum Oxide Template. *J. Cent. South Univ. Technol.* **2011**, *18*, 1004–1008. [CrossRef]
14. Ali, I.; Quazi, M.M.; Zalnezhad, E.; Sarhan, A.A.D.; Sukiman, N.L.; Ishak, M. Hard Anodizing of Aerospace AA7075-T6 Aluminum Alloy for Improving Surface Properties. *Trans. Indian Inst. Met.* **2019**, *72*, 2773–2781. [CrossRef]

15. Kong, D.; Wang, J.; Liu, H. Friction and Wear Performances of 7475 Aluminium Alloy after Anodic Oxidation. *Xiyou Jinshu Cailiao Yu Gongcheng/Rare Met. Mater. Eng.* **2016**, *45*, 1122–1127. [CrossRef]
16. Muthukumar, M.; Yadav, A.; Bobji, M.S. Wear Characteristics of Nanoporous Alumina and Copper Filled Nanocomposite Coatings. *Wear* **2020**, *462–463*, 203496. [CrossRef]
17. Abedini, M.; Hanke, S. Improving the Wear Resistance of Aluminum by a Nickel-Filled Anodized Porous Alumina Layer. *Wear* **2023**, *522*, 204858. [CrossRef]
18. Chen, S.; Kang, C.; Wang, J.; Liu, C.; Sun, K. Synthesis of Anodizing Composite Films Containing Superfine Al_2O_3 and PTFE Particles on Al Alloys. *Appl. Surf. Sci.* **2010**, *256*, 6518–6525. [CrossRef]
19. Escobar, J.; Arurault, L.; Turq, V. Improvement of the Tribological Behavior of PTFE-Anodic Film Composites Prepared on 1050 Aluminum Substrate. *Appl. Surf. Sci.* **2012**, *258*, 8199–8208. [CrossRef]
20. Maejima, M.; Saruwatari, K.; Takaya, M. Friction Behaviour of Anodic Oxide Film on Aluminum Impregnated with Molybdenum Sulfide Compounds. *Surf. Coat. Technol.* **2000**, *132*, 105–110. [CrossRef]
21. Sliney, H.E. The Use of Silver in Self-Lubricating Coatings for Extreme Temperatures. *ASLE Trans.* **1986**, *29*, 370–376. [CrossRef]
22. Shi, X.; Xu, Z.; Wang, M.; Zhai, W.; Yao, J.; Song, S.; ud Din, A.Q.; Zhang, Q. Tribological Behavior of TiAl Matrix Self-Lubricating Composites Containing Silver from 25 to 800 °C. *Wear* **2013**, *303*, 486–494. [CrossRef]
23. Soffritti, C.; Fortini, A.; Nastruzzi, A.; Sola, R.; Merlin, M.; Garagnani, G.L. Dry Sliding Behavior of an Aluminum Alloy after Innovative Hard Anodizing Treatments. *Materials* **2021**, *14*, 3281. [CrossRef] [PubMed]
24. Santecchia, E.; Cabibbo, M.; Hamouda, A.M.S.; Musharavati, F.; Popelka, A.; Spigarelli, S. Dry Sliding Tribological Properties of a Hard Anodized Aa6082 Aluminum Alloy. *Metals* **2020**, *10*, 207. [CrossRef]
25. Nastruzzi, A.; Cicerchia, F.; Fortini, A.; Nastruzzi, C. Gold Hard Anodized (GHA) Materials with Antimicrobial Surface Properties: Mechanical, Tribological, and Microbiological Characterization. *Emergent Mater.* **2021**, *4*, 249–263. [CrossRef]
26. Bahari, A.; Lewis, R.; Slatter, T. Friction and Wear Response of Vegetable Oils and Their Blends with Mineral Engine Oil in a Reciprocating Sliding Contact at Severe Contact Conditions. *Proc. Inst. Mech. Eng. Part J J. Eng. Tribol.* **2018**, *232*, 244–258. [CrossRef]
27. Peña-Parás, L.; Rodríguez-Villalobos, M.; Maldonado-Cortés, D.; González, J.A.; Durán, R.D.J.; Ortega, J.A. Review of Vegetable Nanolubricants for Tribological Applications. *Int. J. Mod. Manuf. Technol.* **2022**, *14*, 333–343. [CrossRef]
28. Luna, F.M.T.; Rocha, B.S.; Rola, E.M.; Albuquerque, M.C.G.; Azevedo, D.C.S.; Cavalcante, C.L. Assessment of Biodegradability and Oxidation Stability of Mineral, Vegetable and Synthetic Oil Samples. *Ind. Crops Prod.* **2011**, *33*, 579–583. [CrossRef]
29. Lee, C.T.; Lee, M.B.; Mong, G.R.; Chong, W.W.F. A Bibliometric Analysis on the Tribological and Physicochemical Properties of Vegetable Oil–Based Bio-Lubricants (2010–2021). *Environ. Sci. Pollut. Res.* **2022**, *29*, 56215–56248. [CrossRef]
30. Fox, N.J.; Stachowiak, G.W. Vegetable Oil-Based Lubricants—A Review of Oxidation. *Tribol. Int.* **2007**, *40*, 1035–1046. [CrossRef]
31. Reeves, C.J.; Menezes, P.L.; Jen, T.C.; Lovell, M.R. The Influence of Fatty Acids on Tribological and Thermal Properties of Natural Oils as Sustainable Biolubricants. *Tribol. Int.* **2015**, *90*, 123–134. [CrossRef]
32. Gerbig, Y.; Ahmed, S.I.U.; Gerbig, F.A.; Haefke, H. Suitability of Vegetable Oils as Industrial Lubricants. *J. Synth. Lubr.* **2004**, *21*, 177–191. [CrossRef]
33. Ruggiero, A.; D'Amato, R.; Merola, M.; Valašek, P.; Müller, M. Tribological Characterization of Vegetal Lubricants: Comparative Experimental Investigation on *Jatropha curcas* L. Oil, Rapeseed Methyl Ester Oil, Hydrotreated Rapeseed Oil. *Tribol. Int.* **2017**, *109*, 529–540. [CrossRef]
34. Rawat, S.S.; Harsha, A.P. The Lubrication Effect of Different Vegetable Oil-Based Greases on Steel-Steel Tribo-Pair. *Biomass Convers. Biorefinery* **2024**, *14*, 1993–2005. [CrossRef]
35. UNI EN 573-3:2024. Available online: https://store.uni.com/en/uni-en-573-3-2024 (accessed on 2 November 2024).
36. Ikeda, T.; Kinju, T.; Matsuo, Y. Method for Surface Treatment of Aluminum or Aluminum Alloys. EU Patent 1207220B1, 16 January 2008.
37. Georgescu, C.; Deleanu, L.; Catalin Cristea, G. Tribological Behavior of Soybean Oil. In *Soybean—Biomass, Yield and Productivity*; IntechOpen: London, UK, 2019.
38. Adhvaryu, A.; Biresaw, G.; Sharma, B.K.; Erhan, S.Z. Friction Behavior of Some Seed Oils: Biobased Lubricant Applications. *Ind. Eng. Chem. Res.* **2006**, *45*, 3735–3740. [CrossRef]
39. Standard Practice for Calculating Viscosity Index from Kinematic Viscosity at 40 °C and 100 °C. Available online: https://www.astm.org/d2270-10r16.html (accessed on 2 November 2024).
40. Straffelini, G. *Friction and Wear: Methodologies for Design and Control*; Springer: Cham, Switzerland, 2015; ISBN 978-3-319-05893-1.
41. Hamrock, B.J.; Dowson, D.; Tallian, T.E. Ball Bearing Lubrication (The Elastohydrodynamics of Elliptical Contacts). *J. Lubr. Technol.* **1982**, *104*, 279–281. [CrossRef]
42. Liu, S.; Peyronnel, A.; Wang, Q.J.; Keer, L.M. An Extension of the Hertz Theory for 2D Coated Components. *Tribol. Lett.* **2005**, *18*, 505–511. [CrossRef]
43. Ortega-álvarez, R.; Hernández-Sierra, M.T.; Aguilera-Camacho, L.D.; Bravo-Sánchez, M.G.; Moreno, K.J.; García-Miranda, J.S. Tribological Performance of 100Cr6/8620 Steel Bearing System under Green Oil Lubrication. *Metals* **2022**, *12*, 362. [CrossRef]
44. Dervishi, E.; McBride, M.; Edwards, R.; Gutierrez, M.; Li, N.; Buntyn, R.; Hooks, D.E. Mechanical and Tribological Properties of Anodic Al Coatings as a Function of Anodizing Conditions. *Surf. Coat. Technol.* **2022**, *444*, 128652. [CrossRef]

45. Ofoegbu, S.U.; Fernandes, F.A.O.; Pereira, A.B. The Sealing Step in Aluminum Anodizing: A Focus on Sustainable Strategies for Enhancing Both Energy Efficiency and Corrosion Resistance. *Coatings* **2020**, *10*, 226. [CrossRef]
46. Yoshikawa, D.S.; Terada, M.; Assis, S.L.; Costa, I.; Padilha, A.F. Correlation between Microstructure and Corrosion Behavior of Two Al-Fe-Si Alloys. *Mater. Corros.* **2016**, *67*, 286–296. [CrossRef]
47. Scampone, G.; Russo, A.; Carminati, A.; Timelli, G. The Influence of the Electrolytic Bath on the Hard Anodizing of Diecast Al–Si–Cu Alloys. *Results Surf. Interfaces* **2022**, *9*, 100089. [CrossRef]
48. Esteban, B.; Riba, J.R.; Baquero, G.; Rius, A.; Puig, R. Temperature Dependence of Density and Viscosity of Vegetable Oils. *Biomass Bioenergy* **2012**, *42*, 164–171. [CrossRef]
49. Guo, B.; Liu, G. Mud Hydraulics Fundamentals. In *Applied Drilling Circulation Systems*; Elsevier: Amsterdam, The Netherlands, 2011; pp. 19–59.
50. Zanini, N.; Suman, A.; Pinelli, M. Experimental Test on Centrifugal Pump Handling Mining Slurries. In *Volume 9: Microturbines, Turbochargers, and Small Turbomachines; Oil and Gas Applications, Proceedings of the ASME Turbo Expo 2023: Turbomachinery Technical Conference and Exposition, Boston, MA, USA, 26–30 June 2023*; American Society of Mechanical Engineers: New York, NY, USA, 2023.
51. Blau, P.J. On the Nature of Running-In. *Tribol. Int.* **2005**, *38*, 1007–1012. [CrossRef]
52. Faes, J.; González, R.; Battez, A.H.; Blanco, D.; Fernández-González, A.; Viesca, J.L. Friction, Wear and Corrosion Behavior of Environmentally-Friendly Fatty Acid Ionic Liquids. *Coatings* **2021**, *11*, 21. [CrossRef]
53. Guicciardi, S.; Melandri, C.; Lucchini, F.; De Portu, G. On Data Dispersion in Pin-on-Disk Wear Tests. *Wear* **2002**, *252*, 1001–1006. [CrossRef]
54. Shibata, K.; Ii, T.; Yamaguchi, T.; Hokkirigawa, K. Tribological Behavior of Polyacetal Composite Filled with Rice Bran Ceramics Particles under Water Lubrication. *J. Compos. Mater.* **2018**, *52*, 2075–2084. [CrossRef]
55. Yamaguchi, T.; Hokkirigawa, K. Friction and Wear Properties of PEEK Resin Filled with RB Ceramics Particles under Water Lubricated Condition. *Tribol. Online* **2016**, *11*, 653–660. [CrossRef]
56. Kerni, L.; Raina, A.; Haq, M.I.U. Friction and Wear Performance of Olive Oil Containing Nanoparticles in Boundary and Mixed Lubrication Regimes. *Wear* **2019**, *426–427*, 819–827. [CrossRef]
57. Luo, X.; Wu, S.; Wang, D.; Yun, Y.; An, Q.; Li, C. Sustainable Development of Cutting Fluids: The Comprehensive Review of Vegetable Oil. *J. Clean. Prod.* **2024**, *473*, 143544. [CrossRef]
58. Mannekote, J.K.; Kailas, S.V. The Effect of Oxidation on the Tribological Performance of Few Vegetable Oils. *J. Mater. Res. Technol.* **2012**, *1*, 91–95. [CrossRef]
59. Johnson, K.L. Contact Mechanics and the Wear of Metals. *Wear* **1995**, *190*, 162–170. [CrossRef]
60. Fouvry, S.; Kapsa, P.; Vincent, L. An Elastic-Plastic Shakedown Analysis of Fretting Wear. *Wear* **2001**, *247*, 41–54. [CrossRef]
61. Kwolek, P.; Krupa, K.; Obłój, A.; Kocurek, P.; Wierzbińska, M.; Sieniawski, J. Tribological Properties of the Oxide Coatings Produced onto 6061-T6 Aluminum Alloy in the Hard Anodizing Process. *J. Mater. Eng. Perform.* **2018**, *27*, 3268–3275. [CrossRef]